1   **dMSCC: A microfluidic platform for microbial single-cell cultivation**

2   **of *Corynebacterium glutamicum* under dynamic environmental**

3   **medium conditions**

4   **Sarah Täuber[1], Corinna Golze[1], Phuong Ho[2], Eric von Lieres[2] and Alexander**

5   **Grünberger[1*]**

6   *[1]Multiscale Bioengineering, Technical Faculty, Bielefeld University, Universitätsstraße*

7   *25, 33615 Bielefeld, Germany*

8   *[2] Institute of Bio- and Geosciences, IBG-1: Biotechnology, Forschungszentrum Jülich,*

9   *52425 Jülich, Germany*

10   ***Correspondence:** alexander.gruenberger@uni-bielefeld.de (A. Grünberger)

11

12   **Keywords**

13   Microfluidics, Single-cell cultivation, *Corynebacterium glutamicum*, Scale-down reactors,

14   Dynamic environments, Lifelines

15

Abstract

In nature and in technical systems, microbial cells are often exposed to rapidly fluctuating environmental conditions. These conditions can vary in quality, e.g., existence of a starvation zone, and quantity, e.g., average residence time in this zone. For strain development and process design, cellular response to such fluctuations needs to be systematically analysed. However, the existing methods for physically emulating rapidly changing environmental conditions are limited in spatio-temporal resolution. Hence, we present a novel microfluidic system for cultivation of single cells and small cell clusters under dynamic environmental conditions (dynamic microfluidic single-cell cultivation (dMSCC)). This system enables to control nutrient availability and composition between two media with second to minute resolution. We validate our technology using the industrially relevant model organism *Corynebacterium glutamicum*. The organism was exposed to different oscillation frequencies between nutrient excess (feasts) and scarcity (famine). Resulting changes in cellular physiology, such as the colony growth rate and cell morphology were analysed and revealed significant differences with growth rate and cell length between the different conditions. dMSCC also allows to apply defined but randomly changing nutrient conditions, which is important for reproducing more complex conditions from natural habitats and large-scale bioreactors. The presented system lays the foundation for the cultivation of cells under complex changing environmental conditions.

Introduction

In large scale industrial cultivations, but also in the natural habitat, microbial cells are exposed to rapidly changing conditions in quality, e.g., existence of a starvation zone, and quantity, e.g., average residence time in this zone.[1–3] These conditions can vary in temperature, oxygen, pH value, shear rate etc. The fluctuating environmental conditions in bioreactors can be caused by long mixing times due to the size of the reactor, the geometry of the reactor (height, diameter, stirrer dimensions, feed inlet location) and the operating mode (stirrer speed, feed rate, gas flow rate). This creates gradients of pH value and nutrients, e.g. substrate concentration and dissolved oxygen concentration.[1] In bioreactors, highly concentrated nutrients are fed regularly, creating different zones of nutrients in the reactor, e.g. zones with substrate excess and zones where no substrates are available. As a result, cells are exposed to different environmental conditions over time, which can be represented by lifelines (recording the environment over time).[4] Typical time scales are in second to minutes range based on the size and geometry of the bioreactor.[5] This has an impact on various variables, which can be divided into biological and technical variables.[6] Biological variables include the influence on cellular metabolism on different cellular levels (transcription, translation)[7,8], while technical variables include for example productivity and yield.[9]

The analysis of cellular behaviour upon defined environmental perturbation on single-cell level is of central interest for the understanding of fundamental topics such as growth rates[10,11], population stability[12] and cellular adaptation[13]. Furthermore, biotechnological questions on the behaviour of single cells in the bioprocess are decisive, e.g., how cells respond to gradients in bioreactors and how cells adapt their gene network upon environmental changes. In order to understand these phenomena, novel methods must be developed, that allow the cultivation of cells at dynamic environmental conditions at the single-cell level.

In recent years, many microfluidic devices have been developed and applied for the cultivation and analysis at single-cell level under defined environmental conditions.[14–16] Here, cells are trapped in different cultivation chamber geometries and perfused with medium. The cultivation chambers on these microfluidic devices range from 0D

69   to 3D systems.[14] For most of the reported single-cell cultivation studies 1D and 2D

70   designs were used. In 1D systems cell growth is enabled in a line of cells upon 4 - 10

71   cells which allows long-term cultivations of small sub-populations. 2D systems allow

72   to cultivate small cell colonies up to 1000 cells in a monolayer.

73   New microfluidic systems are currently being developed for the analysis of cellular

74   behaviour under dynamic environmental conditions.[17,18] The technical setups (pumps

75   and valves) for the generation of dynamic environmental conditions can be

76   implemented outside the microfluidic device (e.g. pressure driven pumps) or

77   integrated into the microfluidic device (e.g. pneumatic valves).[17] Various

78   environmental profiles can be created in these microfluidic systems with different

79   modulation modes. First, the frequency of the pulses can be varied which is called

80   pulse frequency modulation (PFM). Here, the width between the pulses and the

81   amplitude of the pulses are constant. Second, the width of the pulses can be varied,

82   i.e. the time when no new pulse is inserted (pulse width modulation (PWM)). Here,

83   the frequency of the pulses and the amplitude are constant. Third, the amplitude of

84   the pulses can be changed (pulse amplitude modulation (PAM)). Furthermore,

85   random profiles can be generated.

86   In the last years, several microfluidic approaches for studies of cellular physiology at

87   dynamic environmental conditions for microbial cells have been reported (Table 1).

88   Studies with eukaryotic cells are not shown here. Kaiser et al.[19] developed a dial-a-

89   wave system (combination of hardware, software and microfluidic device which

90   include a fluidic mixer) and cultivated *E. coli* cells in mother machine growth channels

91   (1D) with a periodic oscillation of glucose and lactose in 4 hour intervals (PFM-

92   mode). They could show that cells expressed lacZ-GFP from the lac promotor by

93   switching the carbon source from glucose to lactose. Cells completely stopped their

94   growth after three minutes when a switch from glucose to lactose was performed.

95   Rojas et al.[20] used the commercially available microfluidic CellASIC system for the

96   cultivation of *E. coli* cells with a periodic oscillation of LB+sorbitol and LB medium in

97   45 second intervals (PFM-mode). They analysed single-cell behaviour of *E. coli* cells

98   upon hyperosmotic shocks and found that cell elongation is slowed down. When the

99   turgor is restored, the length of the cells recovers. Lugagne et al.[21] cultivated *E. coli*

100   in 1D growth channels with 3.5 h oscillation time including 3 h intervals of LB medium

101   + IPTG and 30 min intervals of LB medium + aTc (PWM-mode). They analysed the

102   gene regulation in a bistable genetic toggle switch in *E. coli* and showed that this can

103   be maintained dynamically. Lambert et al.[22] also cultivated *E. coli* in 1D growth

104   channels with an oscillation between MOPS minimal medium + 0.4% lactose and

105   MOPS minimal medium + 0.4% glucose in 5 minute to 4 hour intervals (PFM-mode).

106   They analysed the non-genetic memory in *E. coli* and showed that the phenotype

107   memory reduced the lag phase under oscillating environment.

108   Most of the demonstrated examples were developed and applied for the investigation

109   of cellular physiology using PFM with intervals between 5 min and hours. Studies

110   with oscillations in seconds to minutes range have not been performed systematically

111   yet for microbial cells. Many studies were designed for eukaryotic cells and yeast and

112   showed a low degree of parallelization of the cultivation chamber. Mostly, complex

113   experimental systems outside the microfluidic device were required such as electrical

114   valves or dial-a-wave-systems. Furthermore, control measurement within the same

115   microfluidic device were technically not implemented before before. Recently, Ho et

116   al.[23] showed that the cultivation of cells with a combination of PWM, PFM and PAM

117   with second scale resolution is challenging, depending on the cultivation chamber

118   design and applied periphery. Thus, systems need to be carefully designed and the

119   feasibility of fast environmental changes needs to be shown for each setup and

120   configuration to guarantee defined medium oscillations.

121

122   Table 1

123

124   In this work, we present a microfluidic single-cell cultivation system for the cultivation

125   of microbial cells under dynamic environmental conditions (dynamic microfluidic

126   single-cell cultivation (dMSCC)). We present a new general microfluidic design/

127   channel layout. Due to the design of the microfluidic system, cells can be cultivated

128   with a high degree of parallelization allowing the collection of statistically meaningful

129   information. The dMSCC setup can create oscillating nutrient profiles between two

130   specified medium conditions, i.e. amount and composition, with a high frequency and
131   thus enables a wide range of experiments with PFM and PWM. The setup allows
132   rapid oscillation of medium for the cultivation and quantitative analysis of single-cell
133   growth at defined environmental conditions with a temporal resolution of seconds (>5
134   seconds). Compared to previously published setups, no integrated or external valves
135   are required for medium oscillations and allow the cultivation of cells without cell loss.
136   Moreover, control measurements of the different medium conditions can be
137   performed. We experimentally characterized the mass transfer during dMSCC and
138   tested the feasibility for realizing controlled oscillating environmental conditions.
139   Furthermore, experimental findings were validated by computational fluid dynamic
140   simulations. The cultivation of *Corynebacterium glutamicum* with different oscillation
141   frequencies between nutrient excess (complex BHI medium) and scarcity (PBS
142   buffer) were performed as a model study. Furthermore, a first proof of concept for the
143   realization of complex environmental profiles as present in bioreactors was
144   demonstrated.

145 **Material and methods**

146 *Pre-cultivation, bacterial strain and growth media*

147 The bacterial strain *C. glutamicum* strain WT ATCC 13032 was used in this study.

148 *C. glutamicum* was cultivated in BHI (Brain heart infusion, Roth, Germany) medium

149 using 37 g L^{-1} BHI at 30 °C. The medium was autoclaved and additionally sterile

150 filtered to prevent channel clogging during the microfluidic experiments.

151 Overnight pre-cultures of *C. glutamicum* were inoculated from glycerol stock in 10 mL

152 BHI medium in 100 mL flasks on a rotary shaker at 120 rpm. Cells from the overnight

153 culture were transferred to inoculate the second culture with a starting OD_{600} of 0.05.

154 When the culture had an OD_{600} of around 0.2 the cells were seeded in the

155 microfluidic device. After seeding, the cells were dynamically perfused with BHI

156 medium and PBS buffer (8 g L^{-1} NaCl, 0.2 g L^{-1} KCl, 1.42 g L^{-1} Na_2HPO_4, 0.27 g L^{-1}

157 KH_2PO_4) according to the protocol description below.

158 *Wafer fabrication*

159 A silicon wafer mould was fabricated with a two-layer photolithography process and

160 served as a mould for PDMS soft lithography.[24] In the following the major processing

161 steps and parameters are described.

162 Photolithography was performed under cleanroom conditions. A 4-inch silicon wafer

163 was cleaned with permonosulphuric acid and demineralised water. Afterwards, the

164 wafer was spin coated and dehydrated through a 15-minute dehydration bake at

165 200 °C. A 800 nm thick layer of negative photoresist SU-8 (18% solid) was spin

166 coated and was pre-baked at 65 °C for 1 minute. Photolithography was performed

167 with a laser beam written 4-inch lithography mask (Deltamask, Netherlands). The

168 exposure time was optimized for the SU-8 thickness, structure resolution and lamp

169 intensity of the mask aligner (MJB3, Süss MicroTec, Germany). Exposure time was

170 set to 1.3 seconds in vacuum contact mode. Furthermore, a 5-minute post-bake at

171 65 °C and 95 °C was performed and the wafer was developed in a negative resist

172 developer (mrdev 600, micro resist technology GmbH, Germany). Afterwards, a

173 second SU-8 layer (52% solid) with a thickness of 10 µm was spin coated onto the

174 wafer. The lithography process was equal to the first layer except the pre-bake

175   process, which was set to 5 minutes at 65 °C and 5 minutes at 95 °C and the
176   exposure time, which was adjusted to 6 seconds.

PDMS Moulding

178   The wafer was covered with PDMS in a ratio 10:1 between base and curing agent
179   (Sylgard 184 Silicone Elastomer, Dow Corning Corporation, USA). Afterwards, the
180   wafer was degassed in an exicator for 30 minutes and baked at 80 °C for 2 hours
181   (universal cupboard, Memmert GmbH, Germany). After this step, the PDMS chips
182   were cut out from the wafer and cleaned three times with isopropanol and blown dry
183   with pressurized air. The cover glasses (D 263 T eco, 39.5x34.5x0.175 mm, Schott,
184   Germany) for the microfluidic chip were also cleaned in this step. Afterwards, the
185   PDMS chip and the cover glass were oxygenised with O_2 plasma (Femto Plasma
186   Cleaner, Diener Electronics, Ebhausen, Germany) for 24 seconds with a power of
187   45% and assembled. Prior the use PDMS-glass bonding was strengthened by a 2-
188   minute bake at 80 °C.

Generation of oscillation profiles

Oscillation setup

191   The microfluidic device was flushed with a cell suspension which was transferred
192   from the main culture at exponential phase with maximum OD_{600} of 0.2. Flow was
193   stopped when enough cultivation chambers were seeded with a single cell (1-4 cells
194   per cultivation chamber). The cell loading process was performed over artificial
195   induced air bubbles in the channels, which temporally change the flow pattern within
196   the microfluidic system. This enables easy, but randomized loading of cells into the
197   monolayer cultivation chambers.[25] Then, the flow was switched from bacterial
198   suspension to growth medium and buffer. Medium flow was achieved with high
199   precision pressure pumps (Line-up series, Fluigent, Jena, Germany) with a pressure
200   of 150 and 75 mbar (flow rate of ~ 6.2 µl/ min for the whole system, leading to a flow
201   rate of around 480 nl/min per cultivation array). Medium was switched with an
202   automated software tool (microfluidic automation tool (MAT), Fluigent, Jena,
203   Germany).

Flow characterisation

205   The flow characterisation within the dMSCC setup was performed with coloured ink

206   (Hardtmuth set of technical inks, Koh-I-Noor, Czech Republic). Different pump

207   settings were tested for the optimal oscillation flow profiles in the microfluidic device.

208   Experimental validation of the mass exchange between supply channels and

209   cultivation chambers was verified with fluorescein (Macrolex yellow, Lanxess,

210   Germany). Medium exchange was characterized by the course of fluorescence upon

211   a change between fluorescein and ethanol. The highest value of the fluorescein

212   signal in a chamber was set to 100% and no fluorescence in the chamber to 0%.

CFD simulations

214   Computational fluid dynamics (CFD) simulations were conducted in COMSOL

215   Multiphysics 5.4.0.225 (COMSOL AB, Sweden). In the CFD model, glucose was

216   used as a representative nutrient, which was specified in the defined CGXII growth

217   medium.[26] Both in the defined medium and in the complex medium the glucose

218   concentration is supersaturated. The maximum substrate concentration was as low

219   as 222 mmol L^{-1}. The stationary velocity field and transient mass transport of glucose

220   were calculated to track the extracellular substrate concentration in the cultivation

221   chamber. The CFD analysis was performed for one representative, empty chamber

222   and for one cultivation chamber filled with a cell colony respectively (see SI Material

223   and Methods). The velocity and concentration fields were sequentially computed and

224   thus the flow field can be regarded as practically independent of the concentration

225   field. For comparison purposes, the medium exchange was described by the course

226   of glucose concentration in the whole cultivation chamber.

Irregular oscillation profiles - lifelines

228   Lifelines simulated by Haringa et al.[4] were chosen to be reproduced by dMSCC.

229   Here, PBS buffer was pulsed on BHI medium. The PBS pulses length varied in all

230   profiles in the following order: 60 sec, 5 sec, 25 sec, 15 sec, 50 sec, 10 sec, 45 sec,

231   30 sec, 60 sec and 5 sec, only the BHI width between theses pulses were varied to

232   generate three different profiles, that differed in the overall medium supply (40% -

233   80%) during the dMSCC.

Time-lapse imaging

Time-lapse microscopy was performed using an inverted automated microscope from Nikon (Nikon Eclipse Ti2, Nikon, Germany). The microscope stage was surrounded with a cage incubator for the optimal temperature control (Cage incubator, OKO Touch, Okolab S.R.L., Italy). The microfluidic device was placed inside the cage incubator in an in-house fabricated chip holder. Additionally, the setup was equipped with an 100x oil objective (CFI P-Apo DM Lambda 100x Oil, Nikon GmbH, Germany), DS-Qi2 camera (Nikon camera DS-Qi2, Nikon GmbH, Germany) and an automated focus system (Nikon PFS, Nikon GmbH, Germany) to compensate the thermal drift during long term microscopy. 60 cultivation chambers were selected manually for each experiment and were managed with NIS-Elements Imaging Software (Nikon NIS Elements AR software package, Nikon GmbH, Germany). Time-lapse images were recorded every 10 minutes.

Data analysis

Data analysis of the live-cell image sequences was performed by using the open source software Fiji[27]. First, a k-mean clustering for the background correction was performed. In the phase contrast images for each time point the cells were separated from the background. The cluster with the cells was retained, the background and the intermediate area between the cells were removed. The cell contours were flattened by morphological operators such as dilatation. Cells which were too close together could not be separated by clustering but were segmented by watershed transformation. Afterwards, the particle analyser was used to obtain the area and the cell count for each time point.

The growth rate was determined by a linear regression through the semi-logarithmic plot of cell numbers over the time. The slope indicates the growth rate.

259 **Results and Discussion**

260 **Device principle and design**

261 The presented microfluidic device (Fig. 1A) was designed for the cultivation and
262 analysis of single cells and cell clusters under dynamic environmental conditions. We
263 designed a chip system containing several arrays of monolayer cultivation chambers,
264 further denoted as cultivation chamber, connected to two medium inlet channels.
265 Each microfluidic chip contains three parallel, separate cultivation units.

266 For the rapid medium oscillation, a new microfluidic channel layout was created.
267 Medium inlet channels are placed at the left and right corner of the 12 cultivation
268 chamber arrays (Fig. 1B). Each cultivation chamber array (a linear series of
269 chambers) has 50 monolayer cultivation chambers. The cultivation chambers are
270 designed as open box chambers based on a previous study from Grünberger et al. [28]
271 and lay the foundation for the dMSCC setup (Fig. 1C). The dimensions of the
272 cultivation chamber are 90 µm x 80 µm and cover an area of around 7200 µm² per
273 cultivation chamber. This enables the cultivation of microcolonies up to several
274 hundred of cells. The cultivation chambers (Fig. 1B green) are around 800 nm in
275 height which restricts cell growth to a monolayer. The flow inside the supply channel
276 is laminar and the mass transfer of nutrients occurs mainly via diffusion inside the
277 cultivation chambers.[25] The arrays are connected to supply channels (Fig. 1B black).
278 The supply channels have a height of around 10 µm and a width of 100 µm.

279

280 Figure 1

281

282 **Dynamic environmental conditions**

283 *Technical Principle*

284 The working principle of our dMSCC system is illustrated in Fig. 2. During dMSCC
285 experiments, medium is switched dynamically between two reservoirs, leading to
286 three distinct cultivation zones (Fig. 2). The two zones are classified as the control
287 zones I & II (left and right) and one zone contains the arrays where medium can be

288   (arbitrarily) changed between the values of the control zones (switching zone). Flow

289   profiles are adjusted in such a way, that always three arrays on the left and right side

290   are control zones and six arrays belong to the switching zone, where cultivation

291   conditions are regulated dynamically. The area where the two liquids converge

292   creates a sharp border layer based on the laminar flow. Fig. 2A shows the flow profile

293   I where nine cultivation chamber arrays are flushed with liquid A and three cultivation

294   chamber arrays as negative control (control zone II) are flushed with liquid B. Fig. 2B

295   shows the flow profile II, where the six cultivation chamber arrays in the centre are

296   perfused with liquid B so that only the positive control (control zone I) is flushed with

297   liquid A. During dMSCC, the system is repeatedly switched between flow profile I and

298   II in specific time-intervals. Fig. 2C and D show the experimental validation of the flow

299   profiles with coloured ink (blue for liquid A and red for liquid B). Furthermore, we

300   tested the spatial reproducibility of the oscillation with a rectangular flow profile

301   between blue and red colour ink in 10 second intervals (see Fig. S1). Here, the

302   deviation (Δx) of the fluid boundaries of the two liquid streams, which are formed by

303   the laminar flow profile, was analysed (see Fig. S1A) and resulted in a deviation from

304   the setpoint $\Delta x = 0$ between $-$ 8 µm and 7 µm (see Fig. S1B). The deviation is most

305   likely caused by the external compressed air fluctuations that are applied to the

306   pressurized pumps. Due to the main channel width of 100µm, the detected deviation

307   of ~ 7 µm can be neglected for the dMSCC experiments.

308

309   Figure 2

310

311   ***Validation of flow profiles and environmental conditions***

312   Detailed flow experiments with fluorescein were performed to validate the setup and

313   the environmental profiles that were obtained during dMSCC. The fluorescence

314   signal of nine cultivation chambers in the different regions of the dMSCC setup (Fig.

315   3A) was analysed with an oscillation between fluorescein and ethanol in 1 minute

316   intervals. The cultivation chambers C1-C3 were in the control zone I of the

317   fluorescein, C4-C7 the switching zone and C8-C9 the control zone II, where no

318 fluorescein was flushed. Fig. 3B shows three representatives cultivation chambers of
319 each zone in the microfluidic device. During these 1-minute oscillation experiments, a
320 fluorescence signal of more than 95% is reached in the cultivation chamber after 5
321 seconds. Additional flow profile characterization experiments were performed with
322 oscillation intervals of 5 seconds and confirmed these findings (see Fig. S2).
323 Depending on the position of the cultivation chamber and thus the flow regime during
324 the switching zone, the exchange rates of fluorescein can slightly differ. For example,
325 cultivation chamber C4 (boundary between two zones) (see Fig. S3 – green curve)
326 shows a faster exchange than the other selected cultivation chambers within the
327 different regions in the arrays (see Fig. S3 – C1-C9). More detailed validation studies
328 with oscillation times up to 0.5 seconds (2 Hz) were performed to test the limitation to
329 realize stable and precise oscillating conditions. Fig. 3C sums up all validation
330 measurements in a Bode plot (experimental results shown in black squares) with
331 different oscillations times between 1 minute (0.017 Hz) and 0.5 second (2 Hz).
332 Smaller oscillation intervals could not be performed due to the technical specification
333 of the pumps. Here, the Bode plot[29] was adapted from electrical engineering. The
334 response is defined as normalized intensity of the fluorescence signal in the
335 cultivation chamber. The plot shows, that medium oscillations up to 5 seconds can be
336 performed, guaranteeing an almost complete medium exchange within the cultivation
337 chamber. At oscillation intervals of 2 seconds (0.5 Hz) the fluorescence signal is 82%
338 so that a full exchange of nutrients cannot be guaranteed anymore at this oscillation
339 frequency. We conclude, for higher frequencies than 0.2 Hz, only a low medium
340 exchange is feasible anymore. At very high oscillation intervals the system showed a
341 transient effect (see Figure S4). At these oscillation frequencies, an average value
342 was determined after the system had settled. At higher oscillation frequencies than 1
343 Hz, the signal in the cultivation chamber decreases only slightly until a stationary
344 state of ~ 50 % is reached.

345 CFD simulations were performed to verify the experimental findings (Fig. 3C – red
346 circles (simulation without a colony) and blue triangles (simulation with a colony as
347 steric hindrance)). The measured substrate concentrations for each frequency are
348 normalized, with the maximum substrate concentration measured in the cultivation
349 chamber in steady state for the lowest frequency denoting 100%. The simulations

350 verify the experimental fluorescence results in the range 0.01 Hz to 2 Hz. Limitation

351 of full medium exchange (~ 98%) can be shown for intervals of 5 seconds (0.2 Hz),

352 which is in good agreement with the respective experimental result. In the case of

353 changes that are greater than 0.5 Hz, a slight offset of the simulation from the

354 experiment can be observed. Above the limit of 0.5 Hz, the simulation shows a faster

355 exchange of the medium compared to the experimental results. The following aspect

356 can explain the discrepancy: The correlation between fluorescein signal and

357 substrate concentration in the cultivation chamber is not impeccably linear, e.g. the

358 height of the respective chamber region on the chip can influence the signal. The

359 influence of the flow rate on substrate exchange was also investigated by simulations

360 with a lower flow rate of 200 nl/ min, i.e. a lower flow rate than in the experimental

361 investigations. No difference was found on substrate exchange in the cultivation

362 chamber. Additionally, the simulations with and without a colony in the cultivation

363 chamber show no significant difference. In case of the simulation with a colony, the

364 substrate diffuses into the free volume with the same velocity. The resulting amount

365 of substance in the free volume is less compared to the one in the empty chamber in

366 case where no colony is simulated, but so is the free volume reduced by the cell

367 colony. That is why, the concentration is virtually constant, and the effect of steric

368 hindrance can be neglected. However, the simulations confirm the operational limits

369 of the dMSCC device.

370 The results show, that dMSCC up to 5 seconds (which corresponds well with

371 environmental changes within bioreactors) can be performed with the presented

372 setup, keeping in mind, that diffusivity of molecules can differ. Furthermore, cell

373 growth within the cultivation chamber can influence diffusion time into the centre of

374 the colonies/ chambers and can have an influence on the available concentration and

375 thus on the substrate uptake.[30]

376

377 Figure 3

378

379

Application – dMSCC of *Coryebacterium glutamicum*

Uniform oscillation profiles - Colony growth

The *C. glutamicum* strain WT ATCC 13032 is an important microbial host for industrial amino acid production[31–33], such as L-lysine[34] and L-glutamate[32]. In the first set of experiments, we investigated the microbial growth under oscillating (rectangular) feast and famine environmental conditions with different uniform oscillation times between 10 seconds and 1 hour (Fig. 4). Oscillation was carried out between the complex BHI medium and phosphate buffer (PBS) at 30 °C under aerobic conditions. The overall ratio between BHI medium (feast) and PBS (famine) was equal in all experiments.

As shown in Fig. 4A, biphasic growth behaviour can be observed at 1 hour oscillation cultivation. During BHI perfusion cells grow exponentially. During the intervals with PBS perfusion, colony growth was interrupted, and cells show no growth at all (Fig. 4A and see the ESI V1). The colony growth rate over the whole cultivation is $\mu_{colony} = (0.37 \pm 0.03)$ h^{-1}. Further experiments with higher oscillation intervals e.g. 45 minute show a similar growth behaviour (see Fig. S6 and the ESI V2). Here, a similar colony growth rate of $\mu_{colony} = (0.32 \pm 0.03)$ h^{-1} was observed. A colony growth rate of $\mu_{colony} = (0.36 \pm 0.04)$ h^{-1} was observed at the 30 minutes oscillations (Fig. 4B and see the ESI V3). At higher oscillation intervals of 5 min (0.003 Hz) to 15 min (0.001 Hz) a growth of $\mu_{colony} = (0.30 \pm 0.01)$ h^{-1} was observed (Fig. 4C and D and see the ESI V4 - V6). Here, colonies show continuous growth in comparison to the low oscillating intervals, which is occasionally interrupted by a clear zero-growth (Fig. 4C and 4D and see Fig. S8 - S10). The 1 minute oscillations of BHI medium and PBS buffer show a faster growth than at the lower oscillation intervals (> 0.003 Hz). Here, a colony growth rate of $\mu_{colony} = (0.49 \pm 0.07)$ h^{-1} was observed (see Fig. S10 and the ESI V7). For faster oscillation intervals of 20 s (0.05 Hz) a growth rate of $\mu_{colony} = (0.58 \pm 0.05)$ h^{-1} was obtained (Fig. 4E and 4F and see the ESI V8 and V9). Under oscillating conditions, a positive influence of frequency on the growth rate was observed from a threshold of 1 minute (0.0167 Hz).

Several types of control experiments were performed with BHI and PBS buffer to guarantee technical functionality of the microfluidic device. The constant perfusion of

411   the cells with BHI resulted in colony growth rates of μ_{colony} = (0.90 ± 0.04) h^{-1}. To

412   exclude that the pressure difference required for the oscillation of the medium has an

413   influence on the colony growth a oscillation between BHI and BHI was performed in

414   10 second oscillation intervals, which resulted in a colony growth rate of

415   μ_{colony} = (0.92 ± 0.02) h^{-1}. These findings show that pressure variation which might

416   result from the medium oscillations have no significant effect on the colony growth

417   rate. As a third control experiment, BHI and PBS were mixed in a ratio of 1:1 to rule

418   out any influence on growth and thus nutrient limitation which could happen by

419   mixing the two components. The cells were continuously cultivated with the 1:1

420   BHI/PBS solution, achieving a colony growth of μ_{colony} = (0.90 ± 0.11) h^{-1}, showing

421   that a pure dilution of the BHI medium has also no effect on the growth rate and

422   physiology of the cells during single-cell cultivation (see Fig. S14A-C).

423

424   Figure 4

425

426   All experiments performed under oscillating environmental conditions show a trend of

427   a decrease in the colony growth rate compared to standard perfusion cultivations. An

428   overview of the different colony growth rates is given in the frequency plot in Fig. 5.

429   At low oscillation intervals (1h, 45min, 30 min), a colony growth rates of

430   μ_{colony} = (0.32 – 0.37) h^{-1} are obtained. Cells respond to changes in the external

431   environment by a complex regulatory system whose aim is the activation of

432   transcription factors controlling the expression of a pool of genes necessary for the

433   adaptation to the new environment.[35,36] This leads to temporal starving environmental

434   conditions and thus growth stop of all cells within the colony (μ_{colony} = (0.03 ± 0.02) h^{-}

435   ^{1}). All cells start to regrow after a medium switch to BHI (data not shown), indicating

436   that cellular viability is maintained during the given starvation phases of each

437   individual cell. The reduced growth rate of μ_{colony} ~ 0.35 h^{-1} can be explained by a

438   biphasic growth, with growth rates of μ_{colony} = (0.65 ± 0.03) h^{-1} during BHI pulse

439   perfusion (non-continuous perfusion), and μ_{colony} ≈ 0 h^{-1} during PBS perfusion (see

440   Fig. S15). We are currently not able to explain the differences in these growth rates

441   μ_{colony} = (0.65 ± 0.03) h^{-1} vs. μ_{colony} = (0.90 ± 0.04) h^{-1} which are obtained during

442   continuous BHI perfusion (see Fig. S14A). We assume, that temporal interruption of
443   cell growth has a significant and temporal ongoing influence on the cellular
444   metabolism and thus on the maximum obtainable growth rates during the BHI growth
445   phases.

446   At oscillation intervals between 5 and 15 minute growth rates show a further
447   significant decrease of the growth rates of μ_{colony} = (0.29 – 0.30) h^{-1} with a (semi-)
448   continuous growth profile. Some colonies show a continuous growth profile (see Fig.
449   S9 – red), while in some colony's distinct non-growth phases were observed (see Fig.
450   S8 - red). Interestingly, the non-growth phases do not agree with the time-intervals of
451   the medium oscillations. During 5 - 15 minute oscillations, the district non-growth
452   phases show larger time-scale (~ 45 min) (see Fig. S8). Currently, we have no
453   detailed explanation for the observed growth phenomena. We suspect that the
454   environmental oscillation in these frequencies have a significant effect onto the gene
455   regulatory network of the cells and might thus result in irregular growth patterns.
456   Another aspect is the storage metabolism, which can be dynamically influenced
457   under oscillating and stationary conditions. This includes the storage carbohydrates
458   and storage pools for e.g. glycolytic intermediates.[37–39] In future, detailed studies and
459   analysis of single-cell behaviour might give further insights into this phenomenon. In
460   comparison, during environmental oscillations at low frequencies, the regulatory
461   network underlies no significant changes over the period of PBS perfusion. At short
462   oscillation intervals (1 min, 20 sec, 10 sec) a continuous growth profile was
463   measured, with a growth rate of μ_{colony} = (0.49 - 0.58) h^{-1}. Cultivation with oscillations
464   between 1 h and 5 min show a significant impairment of the colony growth rate
465   compared to cultivations with short intervals (1 min - 10 sec) and compared to BHI
466   control experiment without oscillation (see Fig. S14A).

467

468   Figure 5

469

470   The reduced growth ranges at intermediate intervals (5 – 15 minute oscillation)
471   cannot be explained conclusively at this time point. We assume, that oscillation

472   intervals interfere with cellular regulation mechanisms which operate as a

473   combination of different levels and stages of the flow of genetic information[40], for

474   example: mRNA degradation (~ 10 min), gene splicing and translated protein (~ one

475   cell generation).[41,42] These processes can only be carried out to a limited extent at

476   high oscillation intervals since only limited new proteins can be encoded during the

477   buffer pulses. There is a positive linear correlation between the RNA/ total protein

478   ratio and the growth rate. More RNA is produced during faster growth, but the protein

479   production rate remains constant. The oscillations can influence this ratio, which

480   means that less RNA is produced and the ratio between RNA and total protein is

481   smaller. The translation efficiency can be achieved by changing the nutrient quality of

482   the medium, so that when the nutrient quality is low, translation is inhibited and the

483   ratio of RNA to total protein is reduced.[43]

484   The growth rates of μ_{colony} = (0.49 - 0.58) h^{-1} found at high oscillation intervals (< 1

485   min) could be explained by differences in metabolism due to oscillations, leading to

486   metabolic adaption rather than regulatory adaptation[44]. Adjustments in metabolism

487   could lead to a change in the energy transformation ATP synthase.[45] When cells use

488   memory mechanisms as survival strategy for long-term cultivation, fitness costs

489   resulting from gene regulatory expression may be reduced after the first stimulus is

490   applied, as in the case of the carbon oscillation by Lambert et al.[22]. This effect can

491   also occur here with the high oscillation frequencies, so that the cells do not have to

492   constantly adapt to the new conditions, which increases the growth rate compared to

493   the lower oscillation frequencies.

494

Uniform oscillation profiles - Single-cell length

496   Besides bulk variables, single-cell variables such as cell length and morphology can

497   be analysed during dMSCC. Looking more detailed into the experimental results

498   shown in the last section (colony growth behaviour), single-cell length distributions

499   were analysed. Fig. 6 shows the cell size distributions for six oscillation frequencies

500   for three colonies with approximately 150 cells after 12 hours of cultivation. There is a

501   large variation of the average and width of the population depending on the

502   oscillation frequency. At the 1 hour oscillation the average cell size of (3.4 ± 0.1) µm

503   was observed. At shorter starvation periods the average cell size decreased so that

504   the 45 minutes oscillation an average cell size of (2.2 ± 0.1) µm, the 30 minutes

505   oscillation an average cell size of (2.0 ± 0.1) µm, the 10 minutes oscillation an

506   average cell size of (2.6 ± 0.1) µm and the 10 seconds oscillation an average cell

507   size of (2.5 ± 0.2) µm were observed (see Fig. S16). The cell length measurement

508   was independent of the choice of the cultivation time, before or after the pulse (see

509   Fig. S17).

510

511   Figure 6

512

513   There is a positive trend between colony growth rate and average cell length. High

514   growth rates lead to significantly increased single-cell cell lengths (Fig. 7). Only the

515   cell length of the one-hour oscillation is outside the linear trend. This correlation

516   between the growth rate and cell size was firstly observed for *Salmonella*

517   *typhimurium* organisms under batch conditions by Schaechter et al.[46].

518

519   Figure 7

520

521

522   **Irregularly oscillating profiles**

523   The dMSCC setup was designed so that medium can be oscillated at high

524   frequencies and with varying lengths (amplitude is constant). To test this feature, first

525   experiments for the reproduction of simulated cellular lifelines[4] of nutrient gradients in

526   large scale bioreactors were performed. In comparison to bioreactor gradients, which

527   are complex and chaotic and not completely understood in the effects of a single cell,

528   here irregular random transitions between feast (BHI-flushed) and famine (PBS-

529   flushed) conditions were performed. We created irregular oscillations with times

530   between 5 seconds and 1 minutes in an coarse-grained analogy of the simulation of

531 lifelines in large scale bioreactors from Haringa et al.[4] (see Fig. S18). The irregular

532 oscillations were varied in the medium supply, the length of PBS buffer pulses was

533 kept constant in all experiments (Fig. 8). Three experiments were performed with

534 different overall medium supply, the first experiment with 40% overall medium supply,

535 the second experiment with 60% overall medium supply and the third experiment with

536 80% overall medium supply during the whole cultivation. The experiments show that

537 the total amount of BHI has a positive influence on the growth rate. We found an

538 exponential correlation (R=0,9999) between the colony growth rate and the total

539 medium supply (see Fig. S19). For 80% overall medium supply over the whole

540 experiment, an overall growth rate of $\mu_{colony} = (0.66 \pm 0.03)$ h^{-1} is shown in Fig. 8C. In

541 experiments with less overall medium supply, an overall growth rate of $\mu_{colony} =$

542 (0.51 ± 0.06) h^{-1} at 60% overall medium supply (Fig. 8B) and an overall growth rate of

543 $\mu_{colony} = (0.42 \pm 0.04)$ h^{-1} at 40% overall medium supply were obtained (Fig. 8A). The

544 results are in agreement, with the results obtained in the uniform oscillation

545 experiments with sub-minute resolution ($\mu \sim (0.49 - 0.58)$ h^{-1}, see Fig. 5), which are

546 performed with a medium supply of 50% during the cultivation time.

547 Our system enables the oscillation of medium compounds. Compared to bioreactors,

548 in which the cells are exposed to changing shear rates, the sole effect of the medium

549 compounds can be investigated. Therefore, the emulation of complex bioreactor

550 cultivation conditions is not directly possible.

551 This lays the foundation for detailed studies of lifelines in bioreactors and the analysis

552 of cellular behaviour under complex fluctuating environmental conditions, e.g., pH

553 value, carbon source and general medium composition.[4] The profiles need to be

554 further optimized, since so far only on/ off profiles can be investigated. Different

555 concentrations/ amplitudes can be simulated with a fast switching back and forth in

556 the sub-second range, when the bacterial cells can perceive the difference between

557 constant conditions and fast changes. In this case any concentration can be

558 simulated by very fast oscillation. Furthermore, microbial interactions can be

559 investigated under oscillating nutrient supply and different pH values.[47]

560

561 Figure 8

562

Conclusions and Outlook

In this work, a new microfluidic single-cell cultivation setup for the cultivation and analysis of microbial single cells at dynamic environmental conditions (dMSCC) with high spatio-temporal resolution was developed. This setup enables fast exchange of medium conditions (in seconds range) as well as simultaneous control measurements of the medium conditions on a chip. Systematic experiments with *C. glutamicum* as a model system were performed with different feast (BHI) and famine (PBS) oscillation intervals between 1 hour and 10 seconds. Our experiments show that cellular growth behaviour was significantly affected at the different oscillating conditions. At low oscillation frequencies ($2.7 \cdot 10^{-4}$ Hz) a colony growth rate of $\mu_{colony} \sim 0.3$ h^{-1} was achieved. As the oscillation frequency increased (0.017 Hz), an increase in growth rates was observed ($\mu_{colony} \sim 0.58$ h^{-1}). Additionally, we demonstrated for the first time the cultivation of microbial cells under mimicked nutrient profiles similar to the environmental conditions present in large-scale bioreactors. With this new system in hand it will be possible to investigate the influence of different feast-famine cycles, different media composition and concentrations on the cellular behaviour at the level of individual microbial cells. This lays the foundation of systematic studies of microbial behaviour at various oscillating environments, both in fundamental and applied microbiology and biotechnology.

582

Author contributions

Conceptualization and investigation: ST, CG and AG. Formal analysis and validation: ST, PH, CG and AG. Visualization: ST and PH. Resources: EL and AG. Supervision: AG. Writing: ST, AG and PH.

587

Conflict of interest

There are no conflict of interest to declare.

590

591 **Acknowledgement**

592 Parts of this work were performed at the cleanroom facilities of the Department of

593 Biophysics and Nanoscience as well as the Department for Physics of

594 Supramolecular Systems and Surfaces at Bielefeld University. The authors would like

595 to thank for all the help and support.

596

References

1. A. R. Lara, E. Galindo, O. T. Ramírez and L. A. Palomares, *Mol Biotech*, 2006, **34**, 355–382. DOI: 10.1385/MB:34:3:355.

2. P. B. Pearman, A. Guisan, O. Broennimann and C. F. Randin, *Trends Ecol Evol*, 2008, **23**, 149–158. DOI: 10.1016/j.tree.2007.11.005.

3. A. P. Sweere, J. R. Mesters, L. Janse, K. C. Luyben and N. W. Kossen, *Biotechnol Bioeng*, 1988, **31**, 567–578. DOI: 10.1002/bit.260310609.

4. C. Haringa, R. F. Mudde and H. J. Noorman, *Biocheml Eng J*, 2018, **140**, 57–71. DOI: 10.1016/j.bej.2018.09.001.

5. F. Käß, I. Hariskos, A. Michel, H.-J. Brandt, R. Spann, S. Junne, W. Wiechert, P. Neubauer and M. Oldiges, *Bioprocess Biosyst Eng*, 2014, **37**, 1151–1162. DOI: 10.1007/s00449-013-1086-0.

6. G. Larsson, M. Trnkvist, E. S. Wernersson, C. Trgrdh, H. Noorman and S.-O. Enfors, *Bioprocess Eng*, 1996, **14**, 281–289. DOI: 10.1007/BF00369471.

7. A. N. Brooks, S. Turkarslan, K. D. Beer, F. Y. Lo and N. S. Baliga, *Wiley Interdiscip Rev Syst Biol Med*, 2011, **3**, 544–561. DOI: 10.1002/wsbm.136.

8. M. Pigllucci, *Trends Ecol Evol*, 1996, **11**, 168–173. DOI: 10.1016/0169-5347(96)10008-2.

9. N. Patel and N. Padhiyar, *Chem Eng Res Des*, 2017, **119**, 160–170. DOI: 10.1016/j.cherd.2017.01.002.

10. C. Dusny, F. S. O. Fritzsch, O. Frick and A. Schmid, *Appl Environ Microbiol*, 2012, **78**, 7132–7136. DOI: 10.1128/AEM.01624-12.

11. S. Klumpp and T. Hwa, *Curr Opin Biotechnol*, 2014, **28**, 96–102. DOI: 10.1016/j.copbio.2014.01.001.

12. R. E. Lenski and M. Travisano, *Proc Natl Acad Sci U S A*, 1994, **91**, 6808–6814. DOI: 10.1073/pnas.91.15.6808.

13. O. Kotte, J. B. Zaugg and M. Heinemann, *Mol Syst Biol*, 2010, **6**, 355. DOI: 10.1038/msb.2010.10.

14. A. Grünberger, W. Wiechert and D. Kohlheyer, *Curr Opin Biotechnol*, 2014, **29**, 15–23. DOI: 10.1016/j.copbio.2014.02.008.

15. F. S. O. Fritzsch, C. Dusny, O. Frick and A. Schmid, *Annu Rev Chem Biomol Eng*, 2012, **3**, 129–155. DOI: 10.1146/annurev-chembioeng-062011-081056.

16. P. Shinde, L. Mohan, A. Kumar, K. Dey, A. Maddi, A. N. Patananan, F.-G. Tseng, H.-Y. Chang, M. Nagai and T. S. Santra, *Int J Mol Sci*, 2018, **19**. DOI: 10.3390/ijms19103143.

17. S. Täuber, E. Lieres and A. Grünberger, *Small*, 2020, 1906670. DOI: 10.1002/smll.201906670.

18. C. Dusny and A. Grünberger, *Curr Opin Biotechnol*, 2019, **63**, 26–33. DOI: 10.1016/j.copbio.2019.11.001.

19. M. Kaiser, F. Jug, T. Julou, S. Deshpande, T. Pfohl, O. K. Silander, G. Myers and E. van Nimwegen, *Nat Commun*, 2018, **9**, 212. DOI: 10.1038/s41467-017-02505-0.

20. E. Rojas, J. A. Theriot and K. C. Huang, *Proc Natl Acad Sci U S A*, 2014, **111**, 7807–7812. DOI: 10.1073/pnas.1402591111.

21. J.-B. Lugagne, S. Sosa Carrillo, M. Kirch, A. Köhler, G. Batt and P. Hersen, *Nat Commun*, 2017, **8**, 1671. DOI: 10.1038/s41467-017-01498-0.

22. G. Lambert, E. Kussell and E. Kussel, *PLoS Genet*, 2014, **10**, e1004556. DOI: 10.1371/journal.pgen.1004556.

23. P. Ho, C. Westerwalbesloh, E. Kaganovitch, A. Grünberger, P. Neubauer, D. Kohlheyer and E. von Lieres, *Microorganisms*, 2019, **7**. DOI: 10.3390/microorganisms7040105.

24. A. Gruenberger, C. Probst, A. Heyer, W. Wiechert, J. Frunzke and D. Kohlheyer, *J Vis Exp*, 2013, 50560. DOI: 10.3791/50560.

25. C. Probst, A. Grünberger, N. Braun, S. Helfrich, K. Nöh, W. Wiechert and D. Kohlheyer, *Anal. Methods*, 2015, **7**, 91–98. DOI: 10.1039/C4AY02257B.

26. S. Unthan, A. Grünberger, J. van Ooyen, J. Gätgens, J. Heinrich, N. Paczia, W. Wiechert, D. Kohlheyer and S. Noack, *Biotechnol Bioeng*, 2014, **111**, 359–371. DOI: 10.1002/bit.25103.

27. J. Schindelin, I. Arganda-Carreras, E. Frise, V. Kaynig, M. Longair, T. Pietzsch, S. Preibisch, C. Rueden, S. Saalfeld, B. Schmid, J.-Y. Tinevez, D. J. White, V. Hartenstein, K. Eliceiri, P. Tomancak and A. Cardona, *Nat Methods*, 2012, **9**, 676–682. DOI: 10.1038/nmeth.2019.

28. A. Grünberger, C. Probst, S. Helfrich, A. Nanda, B. Stute, W. Wiechert, E. von Lieres, K. Nöh, J. Frunzke and D. Kohlheyer, *Cytometry A*, 2015, **87**, 1101–1115. DOI: 10.1002/cyto.a.22779.

29. R. R. Yarlagadda, *Analog and Digital Signals and Systems*, (1st ed.). Springer-Verlag US, Boston, MA, 2010.

30. C. Westerwalbesloh, A. Grünberger, B. Stute, S. Weber, W. Wiechert, D. Kohlheyer and E. von Lieres, *Lab Chip*, 2015, **15**, 4177–4186. DOI: 10.1039/c5lc00646e.

31. M. J. Lee and P. Kim, *Front Microbiol*, 2018, **9**, 2523. DOI: 10.3389/fmicb.2018.02523.

32. J. Becker and C. Wittmann, *Industrial Microorganisms: Corynebacterium glutamicum*. In: *Industrial Biotechnology*. Wiley-VCH Verlag GmbH & Co. KGaA, Weinheim, Germany, 183–220, 2017.

33. L. Eggeling and M. Bott, *Appl Microbiol Biotechnol*, 2015, **99**, 3387–3394. DOI: 10.1007/s00253-015-6508-2.

34. J.-Y. Lee, Y.-A. Na, E. Kim, H.-S. Lee and P. Kim, *J Microbiol Biotechnol*, 2016, **26**, 1341. DOI: 10.4014/jmb.2016.2607.1341.

35. E. Balleza, L. N. López-Bojorquez, A. Martínez-Antonio, O. Resendis-Antonio, I. Lozada-Chávez, Y. I. Balderas-Martínez, S. Encarnación and J. Collado-Vides, *FEMS Microbiol Rev*, 2009, **33**, 133–151. DOI: 10.1111/j.1574-6976.2008.00145.x.

36. L. Cerone and Z. Neufeld, *PLoS ONE*, 2012, **7**, e30283. DOI: 10.1371/journal.pone.0030283.

37. A. Lemoine, N. Maya Martínez-Iturralde, R. Spann, P. Neubauer and S. Junne, *Biotechnol Bioeng*, 2015, **112**, 1220–1231. DOI: 10.1002/bit.25543.

38. W. A. Wilson, P. J. Roach, M. Montero, E. Baroja-Fernández, F. J. Muñoz, G. Eydallin, A. M. Viale and J. Pozueta-Romero, *FEMS Microbiol Rev*, 2010, **34**, 952–985. DOI: 10.1111/j.1574-6976.2010.00220.x.

39. C. A. Suarez-Mendez, A. Sousa, J. J. Heijnen and A. Wahl, *Metabolites*, 2014, **4**, 347–372. DOI: 10.3390/metabo4020347.

40. I. Bervoets and D. Charlier, *FEMS Microbiol Rev*, 2019, **43**, 304–339. DOI: 10.1093/femsre/fuz001.

41. R. Milo and R. Phillips, *Cell biology by the numbers*, (1st ed.). Garland Science, New York, 2016.

42. M. Shamir, Y. Bar-On, R. Phillips and R. Milo, *Cell*, 2016, **164**, 1302-1302.e1. DOI: 10.1016/j.cell.2016.02.058.

43. M. Scott and T. Hwa, *Curr Opin Biotechnol*, 2011, **22**, 559–565. DOI: 10.1016/j.copbio.2011.04.014.

44. C. Bleuven and C. R. Landry, *Proc Biol Sci*, 2016, **283**. DOI: 10.1098/rspb.2016.1458.

45. P. Jurtshuk, *Medical Microbiology*: Bacterial Metabolism, (4th ed.). Galveston, 1996.

46. M. SCHAECHTER, O. MAALOE and N. O. KJELDGAARD, *J Gen Microbiol*, 1958, **19**, 592–606. DOI: 10.1099/00221287-19-3-592.

686   47.   F. Liu, J. Mao, W. Kong, Q. Hua, Y. Feng, R. Bashir and T. Lu, *Nat Commun*, 2020, **11**, 309. DOI:
687   10.1038/s41467-019-13986-6.
688

689   **Figures and Tables**

690   **Table 1**: Overview of different environmental profiles and conditions of microfluidic

691   single-cell cultivation with microbial cells.

Environmental profile (period)	Environmental conditions	Growth chamber design	Application	Ref.
PFM (4 h; 4h)	Glucose; lactose	1D	Analysis of lac operon response in *E. coli*	[19]
PFM (45 sec; 45 sec)	LB; LB medium + sorbitol	2D	Investigation of hyperosmotic shock in *E. coli*	[20]
PWM (3h; 30 min)	LB medium + IPTG; LB medium + aTc	1D	Investigation of gene regulation in *E. coli* (bistable genetic toggle)	[21]
PFM (5 min; 5 min – 4h;4h)	MOPS minimal medium + 0.4% lactose; MOPS minimal medium + 0.4% glucose	1D	Investigation of non-genetic memory in *E. coli*	[22]
PFM + PWM (10sec;10sec – 1h;1h)	BHI medium; PBS buffer	2D	Analysis of growth behaviour in *C. glutamicum*	This work

692

693

694
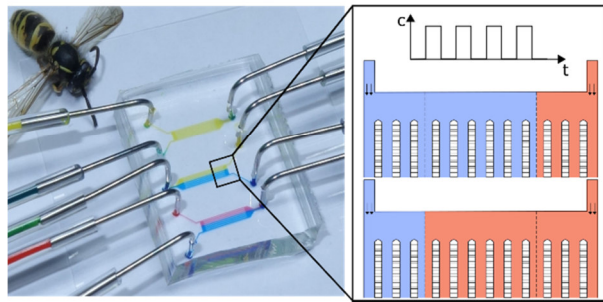
695 **Graphical abstract**

696

697

698
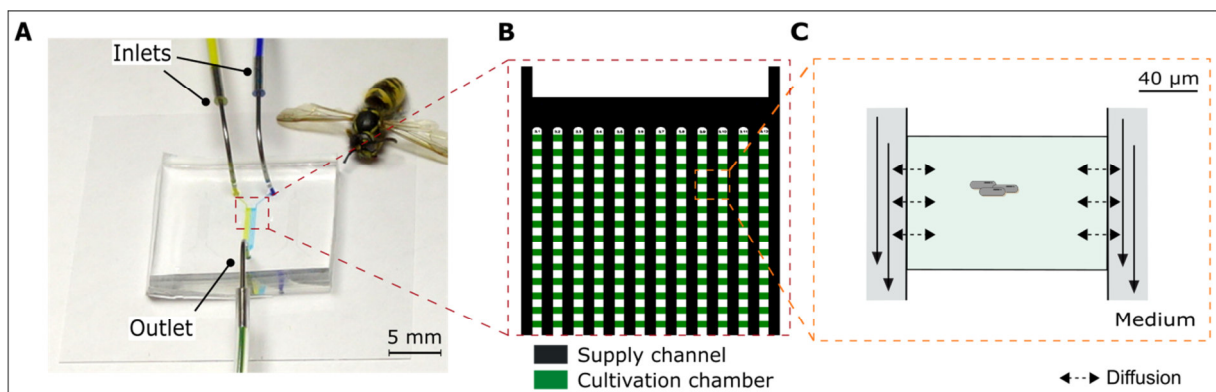
699 **Fig. 1**: Design of the microfluidic chip for cultivation of single cells and small cell

700 clusters under dynamic environmental conditions. A) Microfluidic chip with two inlets

701 and one outlet per cultivation unit. B) Illustration of the 12 arrays of cultivation
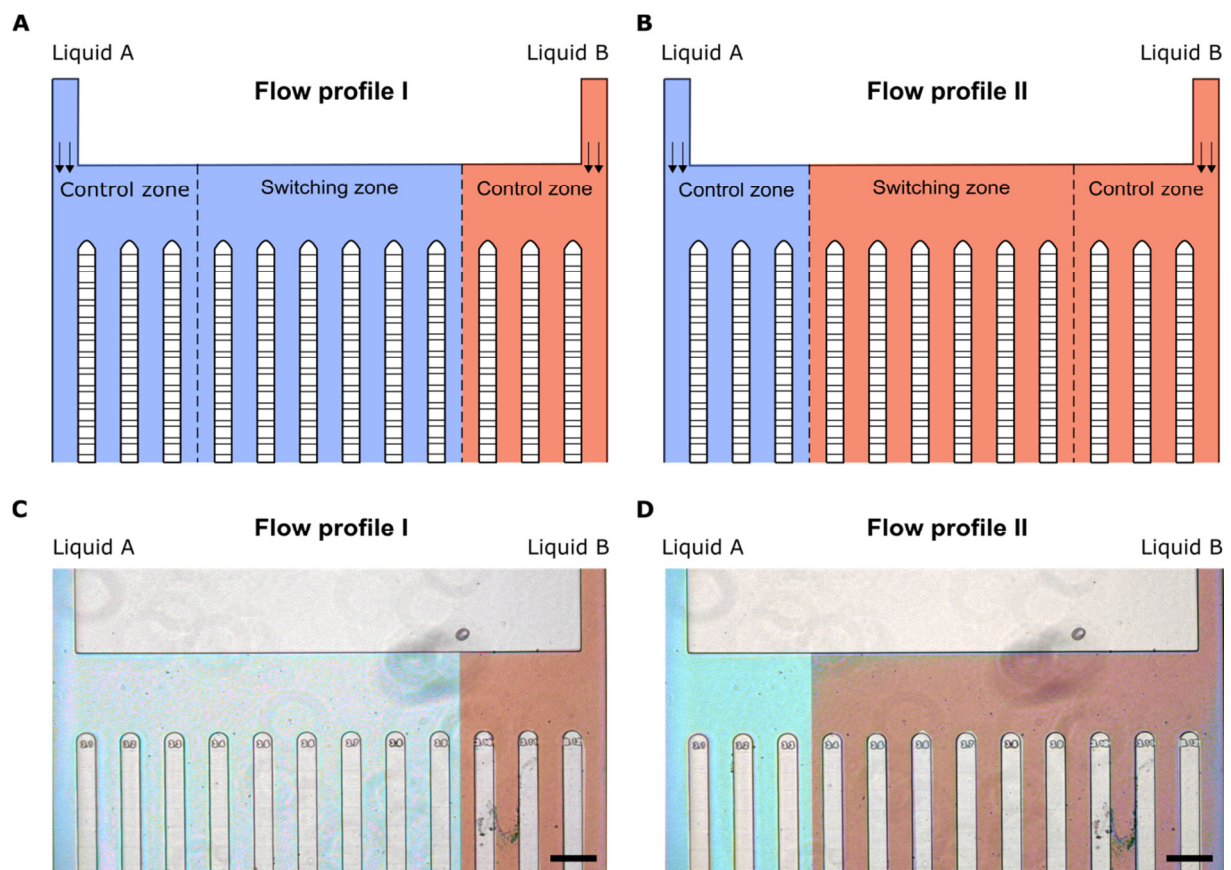
702 chambers. C) Individual monolayer cultivation chamber.

703

Fig. 2: Illustration of the flow profile within the microfluidic dMSCC setup. A) Flow profile I: The six cultivation chamber arrays in the middle are flushed with liquid A. B) Flow profile II: The six arrays in the middle are flush withed the liquid B. C) and D) Microscopic images of the two flow profiles described in A and B. The cultivation chambers are not seen based on the low high of the chambers. Scale bar 200 µm.
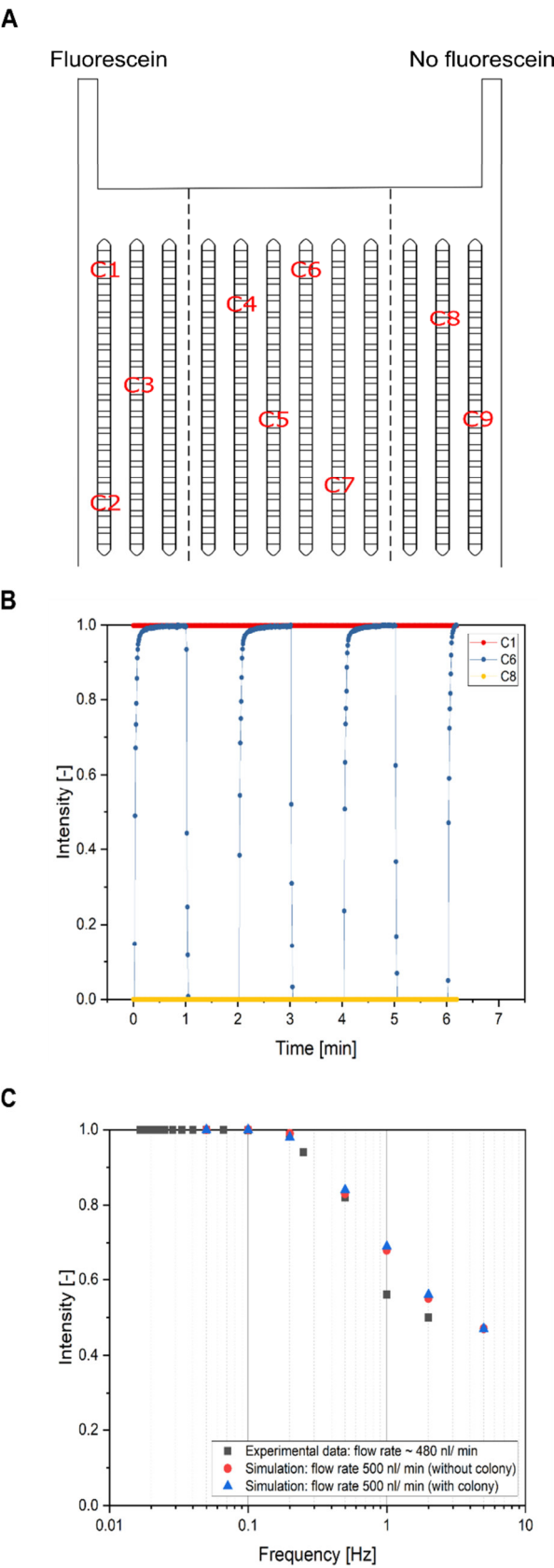
A

B

C

712   **Fig. 3**: Experimental and model-based validation of substrate exchange within single-
713   cell cultivation chambers. A) Schematic overview of the microfluidic device with
714   selected cultivation chambers for the analysis of the fluorescence signal. B)
715   Fluorescence profile of the 1 minute oscillation between fluorescein and ethanol.
716   Here one cultivation chamber from each region in the microfluidic device is shown.
717   Cultivation chamber C1 is in the control zone I (fluorescein region), C6 in the
718   switching zone and C8 in the control zone II (no fluorescein region). C) Bode plot
719   illustrating the fluorescence intensities in the cultivation chambers depending on
720   different oscillation intervals of fluorescein from 100 s (0.01 Hz) to 0.2 s (5 Hz). The
721   experimental validation (black squares) shows the fluorescence signal in cultivation
722   chamber C6. The corresponding CFD simulated concentrations (red circles
723   (simulation without a colony) and blue triangles (simulation with a colony as steric
724   hindrance)) are normalized by the maximum substrate concentration, measured in
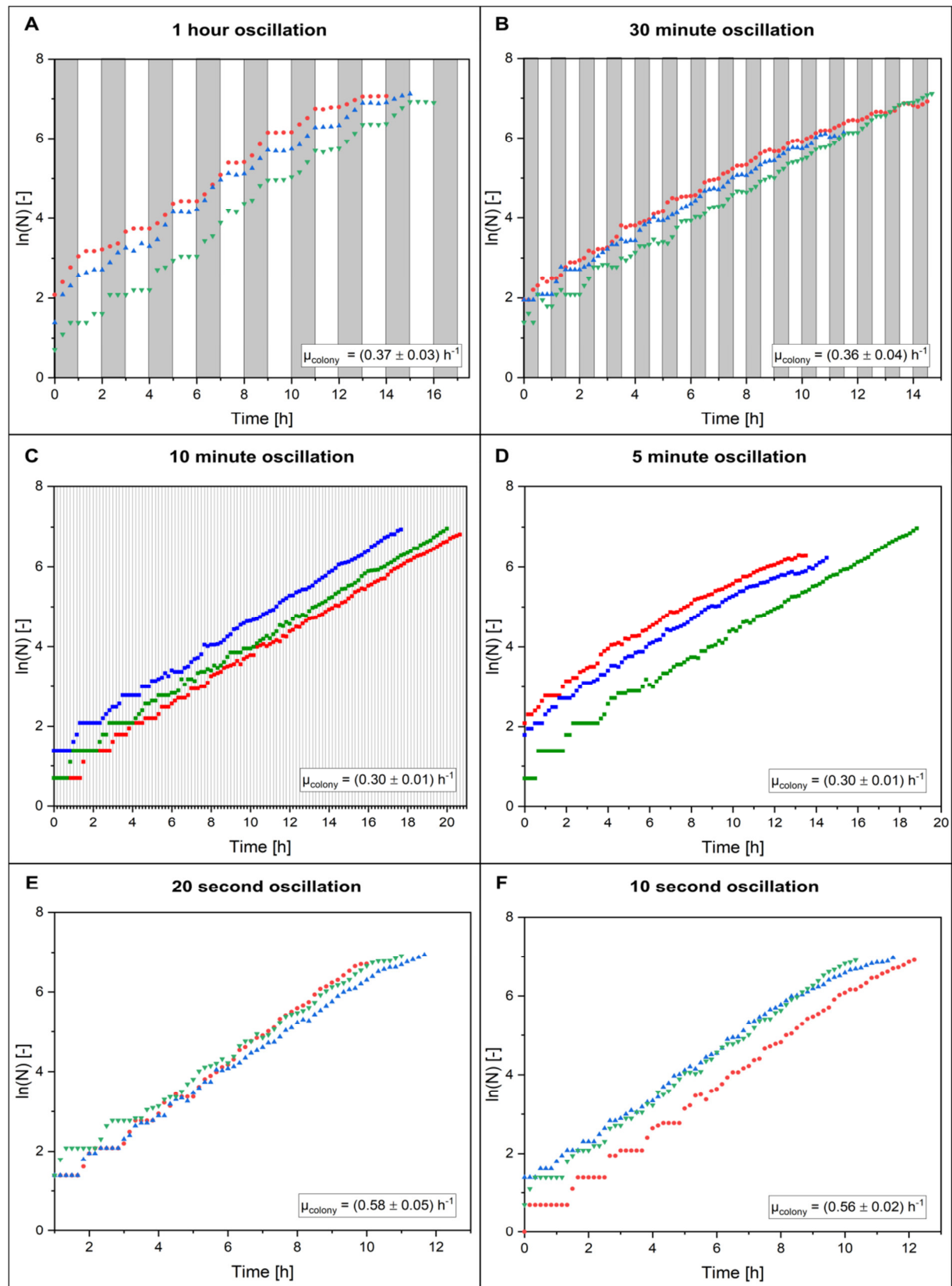725   the cultivation chamber, for the lowest frequency.

726

Fig. 4: Growth curves at different oscillation frequencies between BHI medium and PBS buffer. The grey areas show the BHI medium pulses and the white areas the

730   PBS buffer pulses. At higher oscillation frequencies the different pulse was not

731   shown. A) 1 hour oscillation. B) 30 minute oscillation. C) 10 minute oscillation. D) 5

732   minute oscillation. E) 20 second oscillation. F) 10 second oscillation. Three colonies
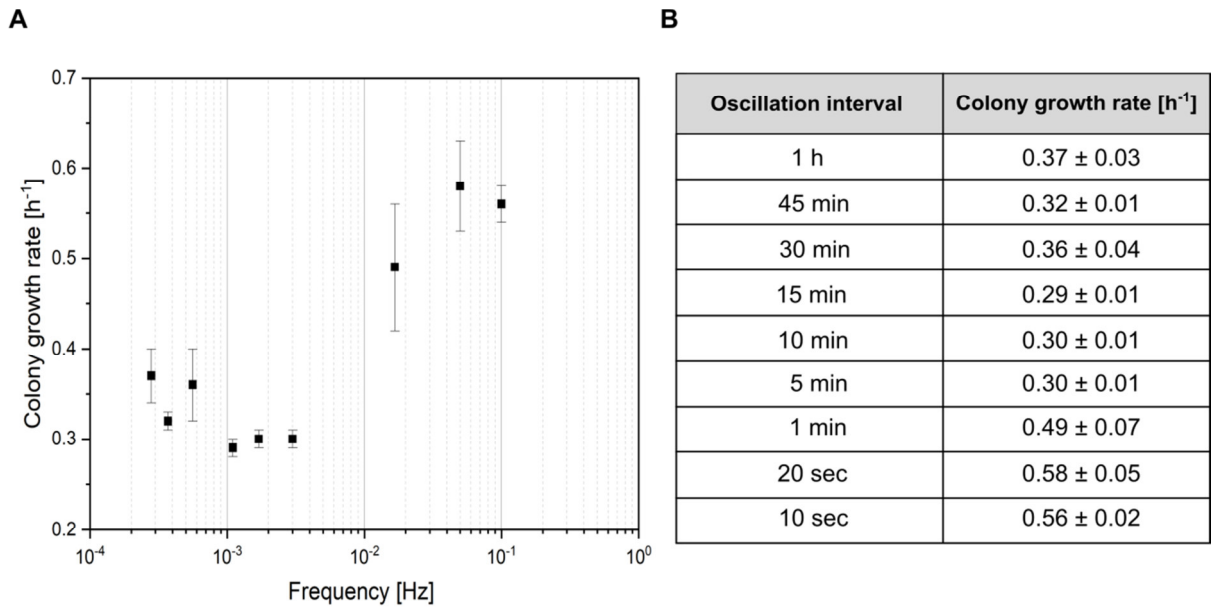
733   (red, green, blue) are shown.

734

735

736   **Fig. 5**: Overview of colony growth rates at varying oscillation frequencies. A)

737   Frequency plot. B) Obtained colony growth rates at different oscillations intervals

738   (N = 8 - 10).

739

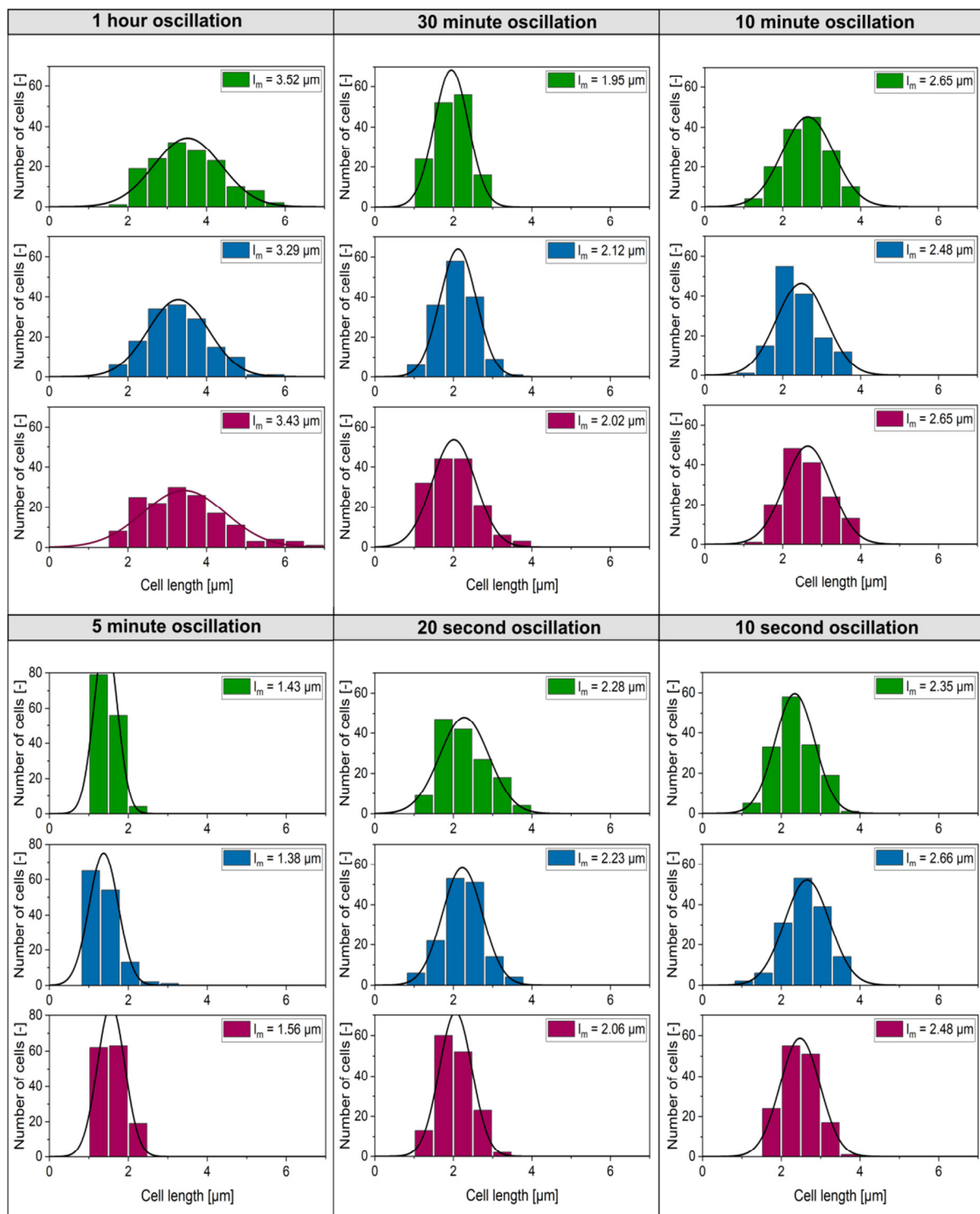| Oscillation interval	Colony growth rate [h^{-1}]
1 h	0.37 ± 0.03
45 min	0.32 ± 0.01
30 min	0.36 ± 0.04
15 min	0.29 ± 0.01
10 min	0.30 ± 0.01
5 min	0.30 ± 0.01
1 min	0.49 ± 0.07
20 sec	0.58 ± 0.05
10 sec	0.56 ± 0.02

Fig. 6: Cell length histogram of the dMSCC with different oscillations frequencies between BHI medium and PBS after 12 h of cultivation, three colonies with N = 150 (green, blue, red).
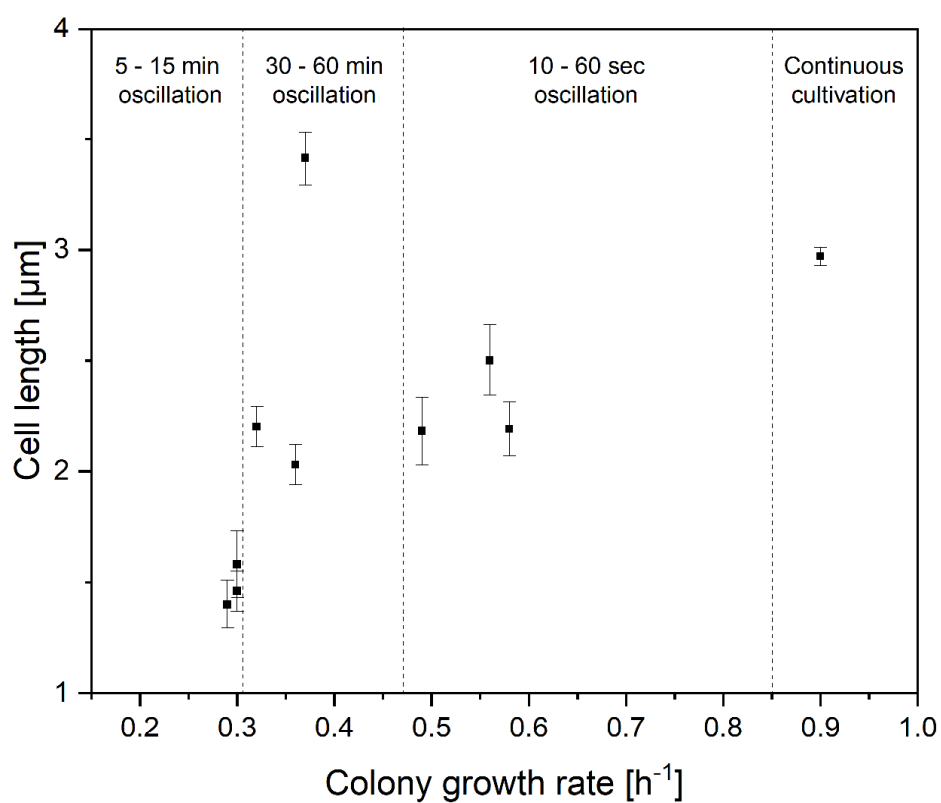
Fig. 7: Colony growth rate from the oscillation cultivation (seen in Fig. 4) as a function of the cell length.
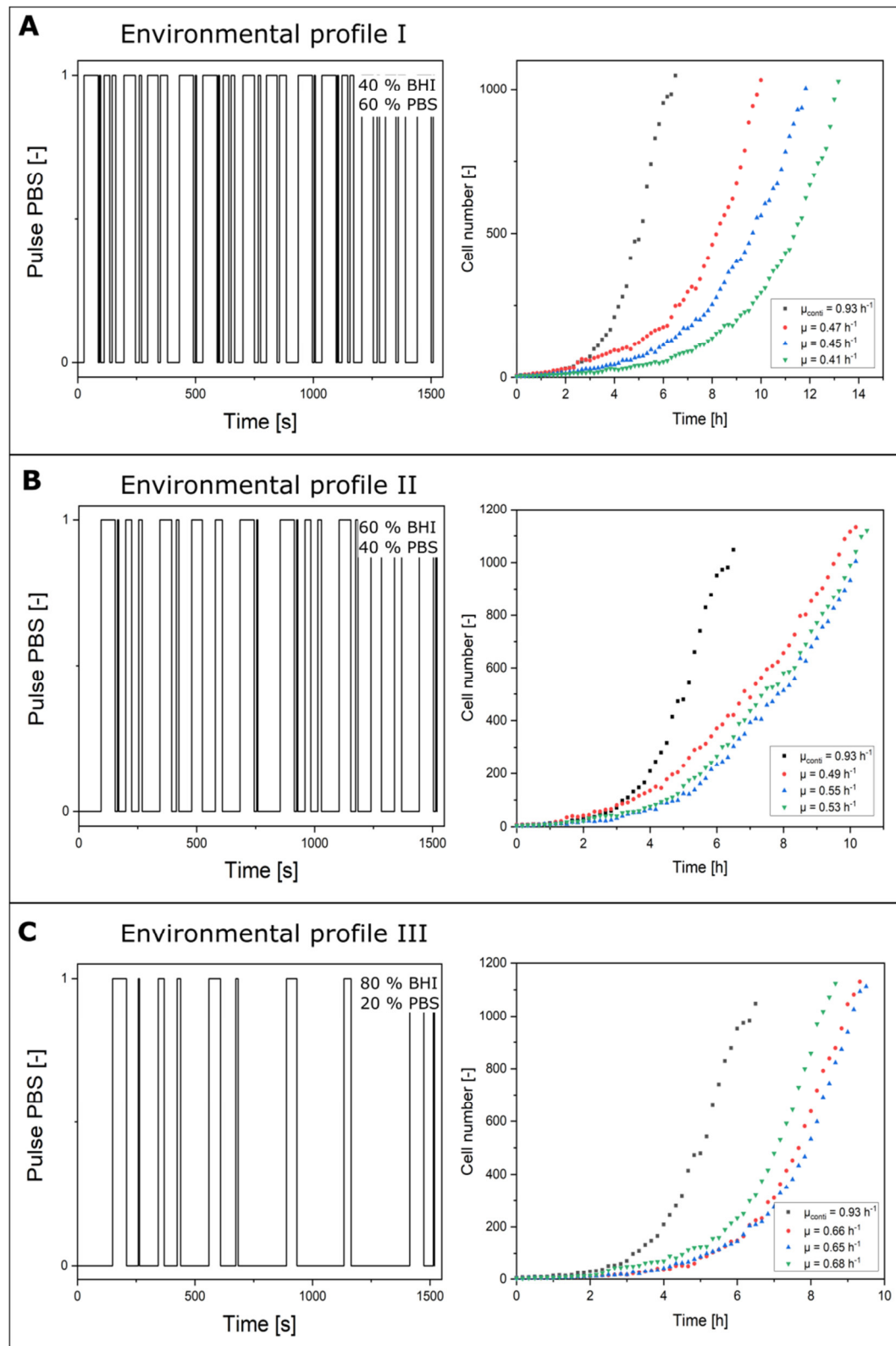
Fig. 8: Feed profiles and measured overall colony growth rates for approximated lifelines with A) 40%, B) 60%, and C) 80% overall medium supply.